J Eng Math (2011) 69:385–400
DOI 10.1007/s10665-010-9406-8

An alternative analytical solution for water-wave motion over a submerged horizontal porous plate

Yong Liu · Yu-cheng Li

Received: 22 November 2009 / Accepted: 5 August 2010 / Published online: 25 August 2010

Abstract This study gives an alternative analytical solution for water-wave motion over an offshore submerged horizontal porous-plate breakwater in the context of linear potential theory. The matched-eigenfunction-expansions method is used to obtain the solution. The solution consists of a symmetric part and an antisymmetric part. The symmetric part is also the solution of wave reflection by a vertical solid wall with a submerged horizontal porous plate attached to it. In comparison with previous analytical solutions with respect to finite submerged horizontal porous plates, no complex water-wave dispersion relations are included in the present solution. Thus, the present solution is easier for numerical implementation. Numerical examples show that the convergence of the present solution is satisfactory. The results of the present solution also agree well with previous results by different analytical approaches, as well as previous numerical results by different boundary-element methods. The present solution can be easily extended to the case of multi-layer submerged horizontal porous plates, which may be more significant in practice for meeting different tide levels.

Keywords Alternative solution · Eigenfunction expansion · Horizontal porous plate · Water wave

1 Introduction

A pile-supported or moored submerged horizontal plate has been proposed as a coastal protection structure since the 1970s [1]. With appropriate design, a submerged horizontal solid plate can reflect the incident wave energy effectively. But when the transmission coefficient attains a minimum, the vertical force acting on the horizontal solid plate is relatively large [2]. To reduce the wave force acting on the plate and dissipate more wave energy, more attention has been given to submerged horizontal porous-plate breakwaters.

Earlier numerical and analytical studies on submerged horizontal porous plates can be found in [2] and [3], respectively. Using the boundary-element method (BEM), Yu and Chwang [2] examined wave motion over an offshore submerged horizontal porous-plate breakwater. They found that a porous plate with suitable porosity could

Y. Liu (✉)
College of Engineering, Ocean University of China, Qingdao 266100, China
e-mail: liuyong_77@hotmail.com

Y. Li
State Key Laboratory of Coastal and Offshore Engineering, Dalian University of Technology, Dalian 116024, China
e-mail: liyuch@dlut.edu.cn

significantly reduce the reflection coefficient and the wave force acting on the plate and still keep the transmission coefficient at a low level. By means of the matched-eigenfunction-expansions method, Chwang and Wu [3] investigated the wave scattering by a submerged horizontal porous circular plate. In their solution, the wave numbers (eigenvalues of depth-dependent eigenfunctions) above and below the horizontal porous plate were the same. The wave numbers were found as a series of complex roots of a complex wave-dispersion relation, which was developed by all the boundary conditions on the free surface, seabed and the porous-plate surface.

Further analytical solutions have also been developed to examine the hydrodynamic performance of different horizontal porous-plate structures, such as: a pitching horizontal porous plate [4], a horizontal porous plate attached to a vertical coastal line [5], a horizontal porous plate of finite thickness [6], a horizontal flexible porous membrane [7], a vertical cylinder with a horizontal porous ring [8], a Jarlan-type perforated breakwater with an internal horizontal porous plate [9] and a submerged breakwater with an upper horizontal porous plate and a lower horizontal solid plate [10]. Among these studies, the one by Neves et al. [6] used experimental data to validate their analytical solution. Also Cho and Kim [7] have validated their analytical solution using the results of a multi-domain BEM solution and experiments. More recently, Kee [11] has used the multi-domain BEM solution and experimental data to examine the hydrodynamic performance of a submerged breakwater composed of a horizontal porous plate and a slightly inclined solid plate. Yueh and Chuang [12] have used a multi-domain BEM solution to examine the reflection coefficient and the wave force on a submerged horizontal or inclined porous plate located above a rubble mound. Bao et al. [13] have developed an analytical solution to calculate the wave forces acting on a submerged porous cylinder including two layers of horizontal porous plates. Besides the structures mentioned above, a submerged horizontal or inclined porous plate can also be installed at the end vertical wall of a wave flume or wave basin in a laboratory, as an effective wave absorber. Studies on this topic can be found in [14,15]. In [15], the analytical solution of diagonal wave reflection by a submerged horizontal porous plate attached to a vertical wall has also been developed. It is noted that in all the above analytical solutions, complex dispersion relations for wave motion over submerged horizontal porous plates were included.

As is well known, an analytical solution can give more scientific insight into the problem. An analytical solution is also easy for numerical implementation. But for previous analytical solutions concerning submerged horizontal porous plates, complex wave-dispersion relations must be solved. This is not at all easy over a range of parameters [16]. Especially for the more significant case of multi-layer horizontal porous plates, the complex wave-dispersion relation will become more involved by including parameters of all the plates. Accurately finding all the complex roots of such an equation is rather difficult, although some solution methods have been developed for complex water-wave-dispersion relations [13,17–19].

More recently, Evans and Peter [16] have developed an explicit solution for the reflection coefficient of a semi-infinite submerged horizontal porous plate by means of the Wiener–Hopf technique. In their solution, no complex wave-dispersion relations were included. Evans and Peter [16] also used the residue-calculus method to determine the reflection coefficient of a submerged horizontal porous plate of finite extent. The complex wave-dispersion relation in the finite porous-plate region still needed to be solved. When being used as a submerged breakwater, the size of the horizontal porous plate along the wave-propagation direction is finite and generally smaller than the incident wavelength. In our present study, an alternative analytical solution for wave motion over an offshore submerged horizontal porous-plate breakwater is developed based on the matched-eigenfunction-expansions method. In comparison with previous studies, the present investigation not only considers the finite extent of the submerged porous plate but also avoids finding the complex roots in the porous-plate region. To the best of our knowledge, this has not been conducted by other researchers so far. The present solution without finding complex roots is easier for numerical implementation. The present solution can also be easily extended to the case of multi-layer submerged horizontal porous plates, which can meet the change of tide level and thus is more significant in practice. In the next section, the boundary-value problem of the present problem is introduced. In Sect. 3, an alternative solution based on the matched-eigenfunction-expansions method is described. In Sect. 4, the convergence of the present solution is examined. The present results are also compared with previous analytical and numerical results. Finally the main conclusions of this study are drawn.

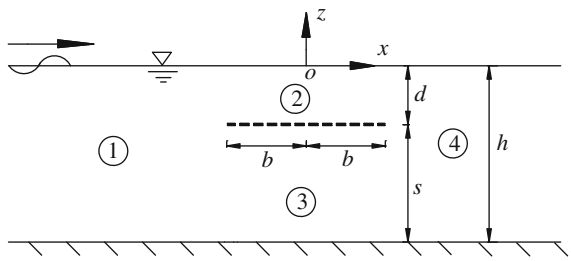

Fig. 1 Sketch of the geometry for a submerged horizontal porous-plate breakwater

2 Mathematical formulation

The idealized geometry of the two-dimensional problem is shown in Fig. 1. A submerged horizontal porous-plate breakwater is located in a water channel of constant depth h. The submerged depth of the porous plate is d. The space between the plate and the seabed is s ($s = h - d$). The length of the plate is $2b$. The submerged porous plate is subject to normally incident regular waves of height H and wavelength L. A Cartesian coordinate system is defined with the origin at the intersection of the plate midline and the still-water level, the x-axis in the direction of wave propagation and the z-axis in the vertical direction upwards. The whole fluid domain is divided into four sub-regions: sub-region 1, the fluid domain at the left-hand side of the plate; sub-region 2, the fluid domain above the porous plate; sub-region 3, the fluid domain beneath the plate; and sub-region 4, the fluid domain at the right-hand side of the plate. Here the thickness of the plate is assumed to be zero, as it is very small in comparison with the water depth and the incident wavelength.

It is assumed that the fluid is inviscid and incompressible, and that the fluid motion is irrotational. Then the fluid motion can be described by a velocity potential $\Phi(x, z, t)$, where t is time. By considering harmonic linear water waves with angular frequency ω, the velocity potential can be written as $\Phi(x, z, t) = \Re\mathfrak{e}[\phi(x, z)\mathrm{e}^{-\mathrm{i}\omega t}]$, where $\Re\mathfrak{e}[\ ]$ denotes the real part of the argument, φ denotes the spatial velocity potential, and $\mathrm{i} = \sqrt{-1}$.

The spatial velocity potentials satisfy the Laplace equation:

$$\frac{\partial^2 \varphi_j(x, z)}{\partial x^2} + \frac{\partial^2 \varphi_j(x, z)}{\partial z^2} = 0, \quad j = 1, 2, 3, 4, \tag{1}$$

where the subscript j represents variables with respect to the sub-region j. Those velocity potentials also satisfy relevant boundary conditions on the free surface, seabed surface and far fields:

$$\frac{\partial \varphi_j}{\partial z} = \frac{\omega^2}{g}\varphi_j, \quad z = 0, \quad j = 1, 2, 4, \tag{2}$$

$$\frac{\partial \phi_j}{\partial z} = 0, z = -h, \quad j = 1, 3, 4, \tag{3}$$

$$\lim_{x \to \pm\infty} \left(\frac{\partial}{\partial x} \mp \mathrm{i}k_0 \right) \begin{pmatrix} \phi_4 \\ \phi_R \end{pmatrix} = 0, \tag{4}$$

where g denotes gravitational acceleration, k_0 is the incident wave number, and ϕ_R is the velocity potential of reflected waves. In addition, the velocity potentials must satisfy matching conditions between different sub-regions:

$$\phi_1 = \begin{cases} \phi_2, & -d \le z \le 0, \\ \phi_3, & -h \le z \le -d, \end{cases} \quad x = -b, \tag{5}$$

$$\frac{\partial \phi_1}{\partial x} = \begin{cases} \frac{\partial \phi_2}{\partial x}, & -d \le z \le 0, \\ \frac{\partial \phi_3}{\partial x}, & -h \le z \le -d, \end{cases} \quad x = -b, \tag{6}$$

$$\phi_4 = \begin{cases} \phi_2, & -d \le z \le 0, \\ \phi_3, & -h \le z \le -d, \end{cases} \quad x = b, \tag{7}$$

$$\frac{\partial \phi_4}{\partial x} = \begin{cases} \frac{\partial \phi_2}{\partial x}, & -d \le z \le 0, \\ \frac{\partial \phi_3}{\partial x}, & -h \le z \le -d, \end{cases} \quad x = b, \tag{8}$$

$$\frac{\partial \phi_2}{\partial z} = \frac{\partial \phi_3}{\partial z} = \mathrm{i}k_0 G(\phi_3 - \phi_2), \quad z = -d, \tag{9}$$

where the symbol G denotes the dimensionless complex porous-effect parameter of the porous plate [20]. When $|G| = 0$, the porous plate reduces to an impermeable plate; while for $|G| \to +\infty$, the plate becomes entirely transparent. Equation (9) is the porous-plate boundary condition [20]. The first equal sign in (9) indicates that the vertical mass fluxes between regions 2 and 3 are continuous at the porous plate. The second equal sign demonstrates that the vertical fluid velocity in the horizontal porous plate is linearly proportional to the pressure difference between the plate's two sides [21]. Details on the porous-effect parameter and the porous-plate boundary can be found in [20] and many other papers [7,9,22–24].

Now (1)–(9) formulate a complete boundary-value problem for linear water-wave motion over a submerged horizontal porous plate. We will solve this problem using an alternative method in the following section.

3 Analytical solutions

To reduce our effort, we split the velocity potential into a symmetric part ϕ^S and an antisymmetric part ϕ^A [25]:

$$\phi(x, z) = \frac{1}{2}\left[\phi^S(x, z) + \phi^A(x, z)\right], \tag{10}$$

where $\phi^S(-x, z) = \phi^S(x, z)$ and $\phi^A(-x, z) = -\phi^A(x, z)$. Now the problem can be solved only in the left half-plane of $x < 0$. To obtain an analytical solution without complex wave-dispersion relations, we further divide the velocity potentials in sub-regions 2 and 3 into two parts as

$$\phi_j^S = \phi_{j,v}^S + \phi_{j,h}^S, \quad j = 2, 3, \tag{11}$$

$$\phi_j^A = \phi_{j,v}^A + \phi_{j,h}^A, \quad j = 2, 3. \tag{12}$$

All the symmetric velocity potentials satisfy the Laplace equation and the following relevant boundary conditions:

$$\begin{cases} \frac{\partial \phi_1^S}{\partial z} = \frac{\omega^2}{g}\phi_1^S, & z = 0, \\ \frac{\partial \phi_1^S}{\partial z} = 0, & z = -h, \\ \lim\limits_{x \to -\infty} \left(\frac{\partial}{\partial x} + \mathrm{i}k_0\right)\phi_R^S = 0, \end{cases} \tag{13}$$

$$\begin{cases} \frac{\partial \phi_{2,v}^S}{\partial z} = \frac{\omega^2}{g}\phi_{2,v}^S, & z = 0, \\ \frac{\partial \phi_{2,v}^S}{\partial z} = 0, & z = -d, \end{cases} \tag{14}$$

$$\frac{\partial \phi_{3,v}^S}{\partial z} = 0, \quad z = -d \quad \text{or} \quad z = -h, \tag{15}$$

$$\begin{cases} \phi_{2,h}^S = 0, & x = -b, \\ \frac{\partial \phi_{2,h}^S}{\partial x} = 0, & x = 0, \\ \frac{\partial \phi_{2,h}^S}{\partial z} = \frac{\omega^2}{g}\phi_{2,h}^S, & z = 0, \end{cases} \tag{16}$$

$$\begin{cases} \phi_{3,h}^S = 0, & x = -b, \\ \frac{\partial \phi_{3,h}^S}{\partial x} = 0, & x = 0. \end{cases} \tag{17}$$

Then, for the symmetric velocity potentials, the matching conditions (5)–(9) can be rewritten as:

$$\phi_1^S = \begin{cases} \phi_{2,v}^S, & -d \le z \le 0, \\ \phi_{3,v}^S, & -h \le z \le -d, \end{cases} \quad x = -b, \tag{18}$$

$$\frac{\partial \phi_1^S}{\partial x} = \begin{cases} \frac{\partial \phi_{2,v}^S}{\partial x} + \frac{\partial \phi_{2,h}^S}{\partial x}, & -d \le z \le 0, \\ \frac{\partial \phi_{3,v}^S}{\partial x} + \frac{\partial \phi_{3,h}^S}{\partial x}, & -h \le z \le -d, \end{cases} \quad x = -b, \tag{19}$$

$$\frac{\partial \phi_{2,h}^{S}}{\partial z}=\frac{\partial \phi_{3,h}^{S}}{\partial z}=\mathrm{i}k_0 G\left(\phi_{3,v}^{S}+\phi_{3,h}^{S}-\phi_{2,v}^{S}-\phi_{2,h}^{S}\right),\quad z=-d. \tag{20}$$

All the antisymmetric velocity potentials satisfy the Laplace equation and the following boundary conditions:

$$\begin{cases}\frac{\partial \phi_1^A}{\partial z}=\frac{\omega^2}{g}\phi_1^A, & z=0,\\ \frac{\partial \phi_1^A}{\partial z}=0, & z=-h,\\ \lim\limits_{x\to-\infty}\left(\frac{\partial}{\partial x}+\mathrm{i}k_0\right)\phi_R^A=0,\end{cases} \tag{21}$$

$$\begin{cases}\frac{\partial \phi_{2,v}^A}{\partial z}=\frac{\omega^2}{g}\phi_{2,v}^A, & z=0,\\ \frac{\partial \phi_{2,v}^A}{\partial z}=0, & z=-d,\end{cases} \tag{22}$$

$$\frac{\partial \phi_{3,v}^A}{\partial z}=0,\quad z=-d\quad\text{or}\quad z=-h, \tag{23}$$

$$\begin{cases}\frac{\partial \phi_{2,h}^A}{\partial x}=0, & x=-b,\\ \phi_{2,h}^A=0, & x=0,\\ \frac{\partial \phi_{2,h}^A}{\partial z}=\frac{\omega^2}{g}\phi_{2,h}^A, & z=0,\end{cases} \tag{24}$$

$$\begin{cases}\frac{\partial \phi_{3,h}^A}{\partial x}=0, & x=-b,\\ \phi_{3,h}^A=0, & x=0.\end{cases} \tag{25}$$

Then, for the antisymmetric velocity potentials, the matching conditions (5)–(9) can be rewritten as:

$$\phi_1^A=\begin{cases}\phi_{2,v}^A+\phi_{2,h}^A, & -d\le z\le 0,\\ \phi_{3,v}^A+\phi_{3,h}^A, & -h\le z\le -d,\end{cases}\qquad x=-b, \tag{26}$$

$$\frac{\partial \phi_1^A}{\partial x}=\begin{cases}\frac{\partial \phi_{2,v}^A}{\partial x}, & -d\le z\le 0,\\ \frac{\partial \phi_{3,v}^A}{\partial x}, & -h\le z\le -d,\end{cases}\qquad x=-b, \tag{27}$$

$$\frac{\partial \phi_{2,h}^A}{\partial z}=\frac{\partial \phi_{3,h}^A}{\partial z}=\mathrm{i}k_0 G\left(\phi_{3,v}^A+\phi_{3,h}^A-\phi_{2,v}^A-\phi_{2,h}^A\right),\quad z=-d. \tag{28}$$

It must be mentioned that the similar conducting method as above was first described by Lee [26] for the heavy radiation of a floating rectangular structure. This can also be found in [27] for wave motion over a submerged bottom-standing rectangular porous bar. Moreover, it can be found in [28] for wave motion over a series of submerged bottom-standing rectangular poro-elastic bars.

By the method of separation of variables, the symmetric velocity potentials that satisfy the Laplace equation and the relevant boundary conditions, (13)–(17), can be written as:

$$\phi_1^S=-\frac{\mathrm{i}gH}{2\omega}\left[\mathrm{e}^{\mathrm{i}k_0(x+b)}Z_0(z)+R_0^S\mathrm{e}^{-\mathrm{i}k_0(x+b)}Z_0(z)+\sum_{n=1}^{\infty}R_n^S\mathrm{e}^{k_n(x+b)}Z_n(z)\right], \tag{29}$$

$$\phi_{2,v}^S=-\frac{\mathrm{i}gH}{2\omega}\left[A_0^S\cos(\lambda_0 x)Y_0(z)+\sum_{n=1}^{\infty}A_n^S\frac{\cosh(\lambda_n x)}{\cosh(\lambda_n b)}Y_n(z)\right], \tag{30}$$

$$\phi_{3,v}^S=-\frac{\mathrm{i}gH}{2\omega}\left[B_0^S X_0(z)+\sum_{n=1}^{\infty}B_n^S\frac{\cosh(\mu_n x)}{\cosh(\mu_n b)}X_n(z)\right], \tag{31}$$

$$\phi_{2,h}^S=-\frac{\mathrm{i}gH}{2\omega}\sum_{n=0}^{\infty}C_n^S W_n^S(x)\frac{\cosh(\beta_n z)+\omega^2/(\beta_n g)\sinh(\beta_n z)}{\cosh(\beta_n d)}, \tag{32}$$

$$\phi_{3,h}^S = -\frac{igH}{2\omega}\sum_{n=0}^{\infty} D_n^S W_n^S(x)\frac{\cosh\beta_n(z+h)}{\cosh(\beta_n s)}, \tag{33}$$

where, R_n^S, A_n^S, B_n^S, C_n^S and D_n^S ($n = 0, 1, 2, \ldots$) are the unknown complex expansion coefficients, and $Z_n(z)$, $Y_n(z)$, $X_n(z)$ and $W_n^S(x)$ ($n = 0, 1, 2, \ldots$) are eigenfunctions as follows:

$$Z_n(z) = \begin{cases} \cosh k_0(z+h)/\cosh(k_0 h), & n = 0, \\ \cos k_n(z+h)/\cos(k_n h), & n = 1, 2, \ldots, \end{cases} \tag{34}$$

$$Y_n(z) = \begin{cases} \cosh \lambda_0(z+d)/\cosh(\lambda_0 d), & n = 0, \\ \cos \lambda_n(z+d)/\cos(\lambda_n d), & n = 1, 2, \ldots, \end{cases} \tag{35}$$

$$X_n(z) = \begin{cases} \sqrt{2}/2, & n = 0, \\ \cos \mu_n(z+h), & n = 1, 2, \ldots, \end{cases} \tag{36}$$

$$W_n^S(z) = \cos(\beta_n x), \quad n = 0, 1, 2, \ldots, \tag{37}$$

in which the eigenvalues k_n and λ_n are the real roots of the following dispersion relations:

$$\omega^2 = gk_0\tanh(k_0 h) = -gk_n\tan(k_n h), \quad n = 1, 2, \ldots, \tag{38}$$

$$\omega^2 = g\lambda_0\tanh(\lambda_0 d) = -g\lambda_n\tan(\lambda_n d), \quad n = 1, 2, \ldots, \tag{39}$$

and the eigenvalues μ_n and β_n are given by

$$\mu_n = \frac{n\pi}{s}, \quad n = 1, 2, \ldots, \tag{40}$$

$$\beta_n = \frac{n+0.5}{b}\pi, \quad n = 0, 1, 2, \ldots. \tag{41}$$

It is noted that the eigenfunctions $Z_n(z)$, $Y_n(z)$, $X_n(z)$ and $W_n^S(x)$ are all orthogonal in their own intervals:

$$\int_{-h}^{0} Z_m(z)Z_n(z)\mathrm{d}z = 0, \quad m \neq n, \tag{42}$$

$$\int_{-d}^{0} Y_m(z)Y_n(z)\mathrm{d}z = 0, \quad m \neq n, \tag{43}$$

$$\int_{-h}^{-d} X_m(z)X_n(z)\mathrm{d}z = 0, \quad m \neq n, \tag{44}$$

$$\int_{-b}^{0} W_m^S(x)W_n^S(x)\mathrm{d}x = 0, \quad m \neq n. \tag{45}$$

The orthogonality will be used to determine the unknown expansion coefficients.

Inserting the expressions for the velocity potentials, (29)–(33), into the matching conditions, (18)–(20), yields:

$$Z_0(z) + \sum_{n=0}^{\infty} R_n^S Z_n(z) = A_0^S\cos(\lambda_0 b)Y_0(z) + \sum_{n=1}^{\infty} A_n^S Y_n(z), \tag{46}$$

$$Z_0(z) + \sum_{n=0}^{\infty} R_n^S Z_n(z) = \sum_{n=0}^{\infty} B_n^S X_n(z), \tag{47}$$

$$ik_0 Z_0(z) + \sum_{n=0}^{\infty} \tilde{k}_n R_n^S Z_n(z)$$

$$= \begin{cases} \sum_{n=0}^{\infty} A_n^S \tilde{\lambda}_n^S Y_n(z) + \sum_{n=0}^{\infty} C_n^S \beta_n \sin(\beta_n b) \frac{\cosh(\beta_n z) + \omega^2/(\beta_n g) \sinh(\beta_n z)}{\cosh(\beta_n d)}, & -d \le z \le 0, \\ \sum_{n=0}^{\infty} B_n^S \tilde{\mu}_n^S X_n(z) + \sum_{n=0}^{\infty} D_n^S \beta_n \sin(\beta_n b) \frac{\cosh \beta_n (z+h)}{\cosh(\beta_n s)}, & -h \le z \le -d, \end{cases} \tag{48}$$

$$\sum_{n=0}^{\infty} C_n^S \left[\omega^2/g - \beta_n \tanh(\beta_n d) \right] W_n^S(x) = \sum_{n=0}^{\infty} D_n^S \beta_n \tanh(\beta_n s) W_n^S(x), \tag{49}$$

$$\sum_{n=0}^{\infty} D_n^S \beta_n \tanh(\beta_n s) W_n^S(x)$$

$$= \mathrm{i}k_0 G \left\{ \begin{array}{l} \sum_{n=0}^{\infty} D_n^S W_n^S(x) - \sum_{n=0}^{\infty} C_n^S \left[1 - \omega^2/(\beta_n g) \tanh(\beta_n d) \right] W_n^S(x) + \frac{\sqrt{2}}{2} B_0^S + \\ \sum_{n=1}^{\infty} B_n^S \cos(\mu_n s) \frac{\cosh(\mu_n x)}{\cosh(\mu_n b)} - A_0^S \frac{\cos(\lambda_0 x)}{\cosh(\lambda_0 d)} - \sum_{n=1}^{\infty} A_n^S \frac{\cosh(\lambda_n x)}{\cosh(\lambda_n b) \cos(\lambda_n d)} \end{array} \right\}, \tag{50}$$

where, $\tilde{k}_0 = -\mathrm{i}k_0, \tilde{k}_n = k_n (n = 1, 2, \ldots), \tilde{\lambda}_0^S = \lambda_0 \sin(\lambda_0 b), \tilde{\lambda}_n^S = -\lambda_n \tanh(\lambda_n b) (n = 1, 2, \ldots), \tilde{\mu}_0^S = 0$ and $\tilde{\mu}_n^S = -\mu_n \tanh(\mu_n b) (n = 1, 2, \ldots)$. Multiplying both sides of (46) by $Y_n(z)$ and integrating with respect to z from $-d$ to 0, then using the orthogonal relation, (43), and truncating n to N, gives a set of linear equations:

$$\left\{ A_n^S \right\} = \left[a_{nm}^S \right] \left\{ R_m^S \right\} + \left[b_n^S \right], \quad n, m = 0, 1, 2, \ldots, N, \tag{51}$$

where the matrix coefficients are given in Appendix A. Multiplying both sides of (47) by $X_n(z)$ and integrating with respect to z from $-h$ to $-d$, then using the orthogonal relation, (44), and truncating n to N, also gives a set of linear equations:

$$\left\{ B_n^S \right\} = \left[c_{nm}^S \right] \left\{ R_m^S \right\} + \left[d_n^S \right], \quad n, m = 0, 1, 2, \ldots, N, \tag{52}$$

where the matrix coefficients can be found in Appendix A. Multiplying both sides of (48) by $Z_n(z)$ and then using a similar method as for (46) and (47) gives another set of linear equations:

$$\left\{ e_m^S \right\} + \left\{ R_m^S \right\} = \left[f_{mn}^S \right] \left\{ A_n^S \right\} + \left[g_{mn}^S \right] \left\{ B_n^S \right\} + \left[h_{mn}^S \right] \left\{ C_n^S \right\} + \left[p_{mn}^S \right] \left\{ D_n^S \right\}, \quad n, m = 0, 1, 2, \ldots, N, \tag{53}$$

in which the matrix coefficients are presented in Appendix A. Multiplying both sides of (49) and (50) by $W_n^S(x)$ and integrating with respect to x from $-b$ to 0, then using the orthogonal relation, (45), and truncating n to N, finally gives two sets of linear equations:

$$\left\{ C_n^S \right\} = \left[q_{nm}^S \right] \left\{ D_m^S \right\}, \quad n, m = 0, 1, 2, \ldots, N, \tag{54}$$

$$\left\{ D_n^S \right\} = \left[r_{nm}^S \right] \left\{ B_m^S \right\} + \left[s_{nm}^S \right] \left\{ C_m^S \right\} + \left[t_{nm}^S \right] \left\{ A_m^S \right\}, \quad n, m = 0, 1, 2, \ldots, N, \tag{55}$$

where the matrix coefficients are also listed in Appendix A. Now all the unknown expansion coefficients in the symmetric potentials can be obtained by solving the linear equations (51)–(55).

By separation of variables, the antisymmetric velocity potentials that satisfy the Laplace equation and the relevant boundary conditions, (21)–(25), can be written as:

$$\phi_1^A = -\frac{\mathrm{i}gH}{2\omega} \left[\mathrm{e}^{\mathrm{i}k_0(x+b)} Z_0(z) + R_0^A \mathrm{e}^{-\mathrm{i}k_0(x+b)} Z_0(z) + \sum_{n=1}^{\infty} R_n^A \mathrm{e}^{k_n(x+b)} Z_n(z) \right], \tag{56}$$

$$\phi_{2,v}^A = -\frac{\mathrm{i}gH}{2\omega} \left[A_0^A \sin(\lambda_0 x) Y_0(z) + \sum_{n=1}^{\infty} A_n^A \frac{\sinh(\lambda_n x)}{\cosh(\lambda_n b)} Y_n(z) \right], \tag{57}$$

$$\phi_{3,v}^A = -\frac{\mathrm{i}gH}{2\omega} \left[B_0^A x X_0(z) + \sum_{n=1}^{\infty} B_n^A \frac{\sinh(\mu_n x)}{\cosh(\mu_n b)} X_n(z) \right], \tag{58}$$

$$\phi_{2,h}^{A} = -\frac{\mathrm{i}gH}{2\omega}\sum_{n=0}^{\infty} C_n^A W_n^A(x)\frac{\cosh(\beta_n z)+\omega^2/(\beta_n g)\sinh(\beta_n z)}{\cosh(\beta_n d)}, \tag{59}$$

$$\phi_{3,h}^{A} = -\frac{\mathrm{i}gH}{2\omega}\sum_{n=0}^{\infty} D_n^A W_n^A(x)\frac{\cosh\beta_n(z+h)}{\cosh(\beta_n s)}, \tag{60}$$

where, $R_n^A, A_n^A, B_n^A, C_n^A$ and $D_n^A (n = 0, 1, 2, \ldots)$ are the unknown complex expansion coefficients, and $W_n^A(x)(n = 0, 1, 2, \ldots)$ are eigenfunctions as follows:

$$W_n^A(x) = \sin(\beta_n x), \quad n = 0, 1, 2, \ldots, \tag{61}$$

in which the eigenvalues $\beta_n (n = 0, 1, 2, \ldots)$ are given in (41). The eigenfunctions $W_n^A(x)$ are orthogonal:

$$\int_{-b}^{0} W_m^A(x) W_n^A(x)\mathrm{d}x = 0, \quad m \neq n. \tag{62}$$

Inserting the expressions for the antisymmetric velocity potentials, (56)–(60), into the matching conditions, (26)–(28), and then using the same conducting methods as for symmetric potentials, yields:

$$\left\{A_n^A\right\} = \left[a_{nm}^A\right]\left\{R_m^A\right\} + \left[h_{nm}^A\right]\left\{C_m^A\right\} + \left[b_n^A\right], \quad n, m = 0, 1, 2, \ldots, N, \tag{63}$$

$$\left\{B_n^A\right\} = \left[c_{nm}^A\right]\left\{R_m^A\right\} + \left[p_{nm}^A\right]\left\{D_m^A\right\} + \left[d_n^A\right], \quad n, m = 0, 1, 2, \ldots, N, \tag{64}$$

$$\left\{e_m^A\right\} + \left\{R_m^A\right\} = \left[f_{mn}^A\right]\left\{A_n^A\right\} + \left[g_{mn}^A\right]\left\{B_n^A\right\}, \quad n, m = 0, 1, 2, \ldots, N, \tag{65}$$

$$\left\{C_n^A\right\} = \left[q_{nm}^A\right]\left\{D_m^A\right\}, \quad n, m = 0, 1, 2, \ldots, N, \tag{66}$$

$$\left\{D_n^A\right\} = \left[r_{nm}^A\right]\left\{B_m^A\right\} + \left[s_{nm}^A\right]\left\{C_m^A\right\} + \left[t_{nm}^A\right]\left\{A_m^A\right\}, \quad n, m = 0, 1, 2, \ldots, N, \tag{67}$$

where the matrix coefficients are all listed in Appendix B. Then the unknown expansion coefficients in the antisymmetric potentials can be obtained by solving the linear equations (63)–(67).

The real reflection and transmission coefficients of an offshore submerged horizontal porous plate, C_R and C_T, can be calculated by:

$$C_R = \frac{\left|R_0^S + R_0^A\right|}{2} \tag{68}$$

$$C_T = \frac{\left|R_0^S - R_0^A\right|}{2} \tag{69}$$

The energy-loss coefficient C_L is defined as

$$C_L = 1 - C_R^2 - C_T^2 \tag{70}$$

For $C_L = 0$, the wave energy has no loss; while for $C_L = 1$, the wave energy is totally dissipated by the porous plate. The spatial dynamic pressure $p(x, z)$ can be obtained by the linear Bernoulli equation:

$$p(x, z) = \mathrm{i}\rho\omega\varphi(x, z) \tag{71}$$

where ρ is the fluid density. Then the magnitude of the vertical wave force acting on the porous plate can be obtained by integrating the dynamic pressure along the plate:

$$F = \mathrm{i}\rho\omega\int_{-b}^{b}(\phi_3-\phi_2)|_{z=-d}\mathrm{d}x = \mathrm{i}\rho\omega\int_{-b}^{0}(\phi_3^S-\phi_2^S)\Big|_{z=-d}\mathrm{d}x = \frac{\rho\omega}{k_0 G}\int_{-b}^{0}\frac{\partial\phi_{3,h}^S}{\partial z}\Big|_{z=-d}\mathrm{d}x$$

$$= \frac{\rho g H}{\mathrm{i}2k_0 G}\sum_{n=0}^{N} D_n^S \sin(\beta_n b)\tanh(\beta_n s) \tag{72}$$

The dimensionless wave force acting on the horizontal porous plate is defined as:

$$C_F = \frac{|F|}{2\rho g H b} \tag{73}$$

As mentioned at the beginning, a submerged horizontal porous plate can be installed at the vertical end wall of a wave flume, as an effective wave absorber. Obviously, the symmetric part of the present solution is just the solution of wave reflection by a vertical solid wall with a submerged horizontal porous plate attached to it (the plate length is b). Then the reflection coefficient of the wave absorber can be calculated by

$$C_R^S = \left| R_0^S \right|. \tag{74}$$

The magnitude of the vertical wave force acting on the porous-plate wave absorber can be calculated by

$$F^S = \mathrm{i}\rho\omega \int_{-b}^{0} (\phi_3^S - \phi_2^S)\,|_{z=-d} \mathrm{d}x \; = F. \tag{75}$$

The dimensionless wave force acting on the horizontal porous plate attached to a vertical wall is defined as:

$$C_F^S = \frac{\left|F^S\right|}{\rho g H b} = \frac{1}{2} C_F \tag{76}$$

We note that our present solution may be further simplified. We can combine the velocity potentials $\phi_{2,\,v}^S$ and $\phi_{3,\,v}^S$ into a single potential $\phi_{23,\,v}^S$, as well as potentials $\phi_{2,\,v}^A$ and $\phi_{3,\,v}^A$ into a single potential $\phi_{23,\,v}^A$. Then the boundary conditions (14) and (15) and the boundary conditions (22) and (23) are, respectively, reduced to

$$\begin{cases} \frac{\partial \phi_{23,\,v}^S}{\partial z} = \frac{\omega^2}{g} \phi_{23,\,v}^S, & z = 0, \\ \frac{\partial \phi_{23,\,v}^S}{\partial z} = 0, & z = -h, \end{cases} \tag{77}$$

$$\begin{cases} \frac{\partial \phi_{23,\,v}^A}{\partial z} = \frac{\omega^2}{g} \phi_{23,\,v}^A, & z = 0, \\ \frac{\partial \phi_{23,\,v}^A}{\partial z} = 0, & z = -h. \end{cases} \tag{78}$$

The two new velocity potentials instead of the potentials given in (30), (31), (57) and (58) can be written as

$$\phi_{23,v}^S = -\frac{\mathrm{i}gH}{2\omega} \left[E_0^S \cos(k_0 x) Z_0(z) + \sum_{n=1}^{\infty} E_n^S \frac{\cosh(k_n x)}{\cosh(k_n b)} Z_n(z) \right], \tag{79}$$

$$\phi_{23,v}^A = -\frac{\mathrm{i}gH}{2\omega} \left[E_0^A \sin(k_0 x) Z_0(z) + \sum_{n=1}^{\infty} E_n^A \frac{\sinh(k_n x)}{\cosh(k_n b)} Z_n(z) \right], \tag{80}$$

where E_n^S and E_n^A ($n = 0, 1, 2, \ldots$) are complex unknown expansion coefficients. Now all the unknown coefficients reduce to four groups, which can also be obtained using the same method as above. But we have found in our calculations that the convergence of the latter method was not fast. Thus it is not detailed here.

It can be seen that, to obtain the solution, we combined two techniques: symmetric and antisymmetric potentials with respect to the vertical axis; and both horizontal and vertical eigenfunction expansions in the regions above and below the plate. Using double eigenfunctions avoids finding complex roots. Using symmetric and antisymmetric potentials effectively reduces the size for the system of truncated equations. This can save effort in the solution procedure, especially when extending the present solution to the case of multi-layer plates. It seems that these two techniques are first combined in this study. Thus, the boundary conditions, (16), (17), (24) and (25), and the relevant potentials, (32), (33), (59) and (60), have all been newly developed. For the linear problem, the velocity potential and the boundary conditions can be linearly split as required. The linear sums of our new artificial potentials still satisfy the Laplace equation and all the original boundary conditions. This should be the reason why the present method works.

Table 1 Convergence of C_R and C_T with increasing values of N at $G=1.0$, $b/h=0.5$, $d/h=0.2$ and different k_0d

N	$k_0d=0.5$		$k_0d=1.0$		$k_0d=2.0$		$k_0d=4.0$		$k_0d=8.0$	
	C_R	C_T	C_R	C_T	C_R	C_T	C_R	C_T	C_R	C_T
5	0.037	0.979	0.169	0.843	0.240	0.617	0.056	0.566	0.025	0.796
10	0.038	0.978	0.170	0.841	0.240	0.613	0.058	0.562	0.028	0.795
20	0.038	0.978	0.171	0.839	0.239	0.611	0.059	0.560	0.028	0.794
40	0.038	0.978	0.172	0.839	0.238	0.610	0.059	0.559	0.028	0.793
60	0.038	0.977	0.172	0.838	0.238	0.609	0.060	0.559	0.028	0.793
100	0.039	0.977	0.172	0.838	0.238	0.609	0.060	0.559	0.028	0.793

Also, it should be mentioned that the square-root singularity of the gradient of the potentials at the tip of the porous plate (see [16, Eq. 1e], [29, p. 40]) are not considered in the present solution. Generally two methods may be considered to incorporate the singularity near the edges of finite plates: the residue-calculus method [29, Chap. 5.2] and the multi-term Galerkin method [30]. The residue-calculus method has been used for a finite-surface fixed horizontal plate and periodic coastlines [29, Chap. 5.2] and a finite submerged horizontal porous plate [16]. The multi-term Galerkin method has been widely used for various vertical thin or thick barriers with gaps, oscillatory water-column devices, periodic arrays of breakwaters and step topography [31–33]. But we have no idea how to incorporate the singularity in our present solution with five unknown potentials. Although the singularity was not considered, the predicted results of the present solution have acceptable accuracy for engineering purposes. This will be shown in the following section.

4 Validation with discussion

To validate the alternative method, we have written a computer procedure to implement the above analytical solution. The convergence of the present solution with the increasing value of truncation number N has been examined. The predicted values of the reflection coefficient, the transmission coefficient, the energy-loss coefficients and the dimensionless wave force have also been compared with previous results of various researchers [2,4,7,10,15]. Also, the singularities near the edges of the finite plates were not considered in the solutions of these researchers.

The calculated results for the reflection and transmission coefficients with different N-values are listed in Tables 1, 2, 3 and 4. Here the four typical basic parameters used in the calculations are $k_0d = 2.0$, $G = 1.0$, $b/h = 0.5$ and $d/h = 0.2$. In each table, one selected parameter is varied over a wide range, and the remaining three parameters are fixed. It can be seen from these tables that the convergence of the present solution is acceptable. Generally, a value of $N = 40$ is sufficient to ensure accurate results for engineering purposes. This is why the value of $N = 40$ was adopted in the present study.

The analytical solutions of Yip and Chwang [4], Cho and Kim [7] and Liu et al. [10] can also be used to calculate the hydrodynamic parameters of a submerged horizontal porous plate. In their solutions, the eigenvalues (wave numbers) of depth-dependent eigenfunctions above and below the porous plate were the same, and the complex wave-dispersion relations must be solved. Comparisons between the present method and those of Yip and Chwang [4], Cho and Kim [7] and Liu et al. [10] are given in Figs. 2, 3 and 4, respectively. In these figures, the lines represent the results calculated by the present method, whereas the symbols are for the results of previous studies. In Fig. 2, the calculation conditions are $d/h = 0.3$, $k_0h = 0.5\pi$ and $b/L = 0.2$. Here each dimensionless coefficient is plotted as a function of the porous-effect parameter G on a logarithmic scale (Here a real G is used). In Fig. 3, the calculation conditions are $d/h = 0.1$, $G = 1.0/\pi$ and $b/h = 0.3$ and 0.5. In this figure, only the transmission coefficient is compared, as the other dimensionless coefficients were not presented in [7]. As for Fig. 4, the values used are $d/h = 0.2$, $k_0h = 1.5$ and $G = 1.0$. From Figs. 2, 3 and 4, it is evident that the agreement between

Table 2 Convergence of C_R and C_T with increasing values of N at $k_0 d = 2.0$, $b/h = 0.5$, $d/h = 0.2$ and different G

N	$G = 0.0$		$G = 0.5$		$G = 1.0$		$G = 5.0$		$G = 10.0$	
	C_R	C_T	C_R	C_T	C_R	C_T	C_R	C_T	C_R	C_T
5	0.756	0.655	0.383	0.535	0.240	0.617	0.060	0.874	0.031	0.933
10	0.760	0.649	0.382	0.530	0.240	0.613	0.060	0.874	0.031	0.933
20	0.761	0.648	0.381	0.527	0.239	0.611	0.060	0.874	0.031	0.933
40	0.762	0.648	0.380	0.525	0.238	0.610	0.060	0.874	0.031	0.933
60	0.762	0.648	0.380	0.525	0.238	0.609	0.060	0.874	0.031	0.933
100	0.762	0.648	0.380	0.524	0.238	0.609	0.060	0.874	0.031	0.933

Table 3 Convergence of C_R and C_T with increasing values of N at $k_0 d = 2.0$, $G = 1.0$, $d/h = 0.2$ and different b/h

N	$b/h = 0.1$		$b/h = 0.5$		$b/h = 1.0$		$b/h = 2.0$		$b/h = 4.0$	
	C_R	C_T	C_R	C_T	C_R	C_T	C_R	C_T	C_R	C_T
5	0.040	0.988	0.240	0.617	0.079	0.231	0.075	0.021	0.058	0.068
10	0.040	0.987	0.240	0.613	0.081	0.230	0.079	0.022	0.076	0.004
20	0.042	0.986	0.239	0.611	0.082	0.228	0.080	0.022	0.079	0.001
40	0.043	0.985	0.238	0.610	0.082	0.228	0.080	0.022	0.079	0.000
60	0.043	0.985	0.238	0.609	0.082	0.228	0.080	0.022	0.080	0.000
100	0.043	0.984	0.238	0.609	0.082	0.228	0.080	0.022	0.080	0.000

Table 4 Convergence of C_R and C_T with increasing values of N at $k_0 d = 2.0$, $G = 1.0$, $b/h = 0.5$ and different d/h

N	$d/h = 0.05$		$d/h = 0.1$		$d/h = 0.2$		$d/h = 0.5$		$d/h = 0.95$	
	C_R	C_T	C_R	C_T	C_R	C_T	C_R	C_T	C_R	C_T
5	0.241	0.358	0.255	0.401	0.240	0.617	0.080	0.900	0.001	0.999
10	0.242	0.355	0.251	0.393	0.240	0.613	0.081	0.898	0.001	0.999
20	0.242	0.355	0.250	0.391	0.239	0.611	0.081	0.897	0.001	0.999
40	0.242	0.354	0.249	0.389	0.238	0.610	0.081	0.897	0.001	0.999
60	0.242	0.354	0.249	0.388	0.238	0.609	0.081	0.896	0.001	0.999
100	0.242	0.354	0.248	0.388	0.238	0.609	0.081	0.896	0.001	0.999

the present predictions and previous results obtained by different analytical approaches is very good. It can also be seen from these figures that a submerged horizontal suitably designed porous plate can be used as an effective coastal-protection structure.

The present results for C_R, C_T, C_L and C_F are also compared with the numerical results of Yu and Chwang [2], as shown in Fig. 5. The results of Yu and Chwang [2] were calculated by a BEM solution. The fundamental solution of the Laplace equation used by them satisfied all the boundary conditions on the free surface, seabed and far fields. It can be seen from Fig. 5 that the agreement between the present method and that of Yu and Chwang [2] is good. It can also be seen from this figure that constructing a horizontal porous-plate breakwater near the free surface is more effective, as indicated by Yu and Chwang [2].

For a submerged horizontal porous-plate wave absorber attached to a vertical solid wall, Cho and Kim [15] have calculated the reflection coefficient C_R^S of the structure, using both an analytical solution and a simple source-based

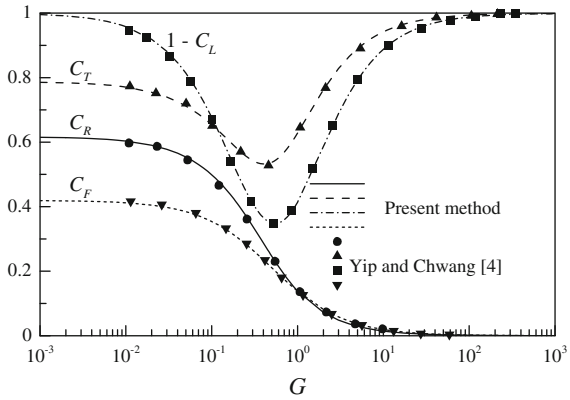

Fig. 2 Comparison between the present method and that of Yip and Chwang [4]: $d/h = 0.3$, $k_0h = 0.5\pi$ and $b/L = 0.2$

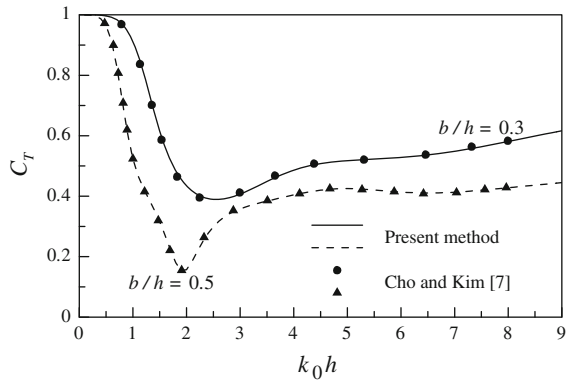

Fig. 3 Comparison between the present method and that of Cho and Kim [7]: $d/h = 0.1$ and $G = 1.0/\pi$

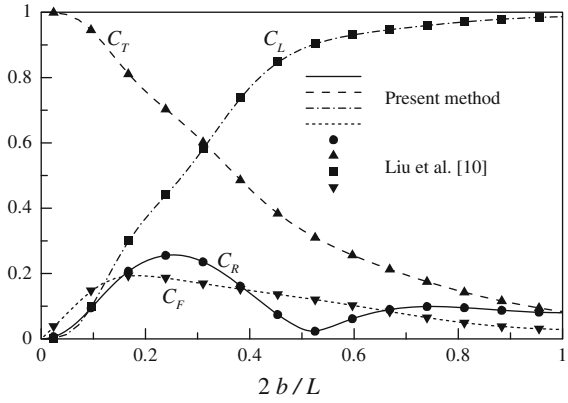

Fig. 4 Comparison between the present method and that of Liu et al. [10]: $d/h = 0.2$, $k_0h = 1.5$, and $G = 1.0$

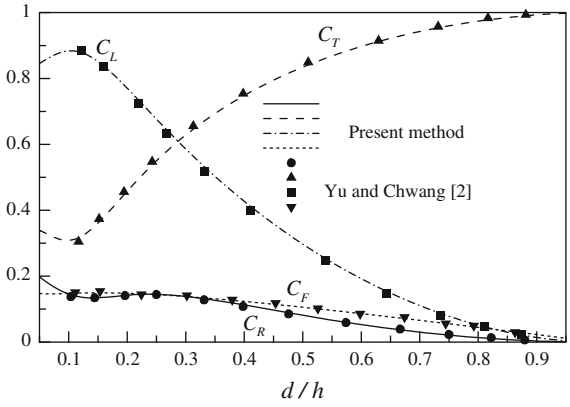

Fig. 5 Comparison between the present method and that of Yu and Chwang [2]: $b/h = 0.8$, $k_0h = 0.5\pi$, and $G = 1.0$

Fig. 6 Comparison between the present method and that of Cho and Kim [15]: $b/h = 1.0$ and $G = 2.5/\pi$

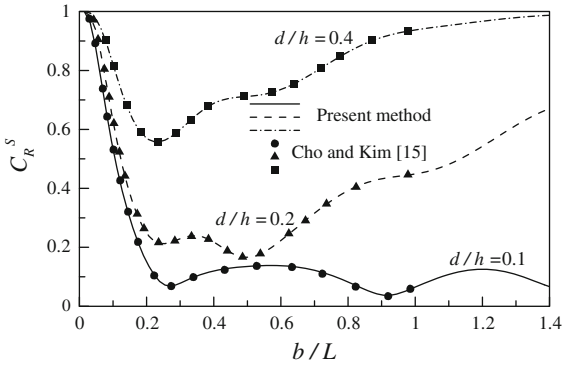

multi-domain BEM solution. In their analytical solution, the wave numbers above and below the plate were the same, which was basically the same as the findings of Yip and Chwang [4], Cho and Kim [7] and Liu et al. [10]. Figure 6 shows a comparison between the present method and the analytical solution of Cho and Kim [15] for $b/h = 1.0$, $G = 2.5/\pi$ and $d/h = 0.1, 0.2$ and 0.4. It is evident from Fig. 6 that the reflection coefficients

given by the two different analytical methods agree very well. Moreover, our present results also agree well with the multi-domain BEM results of Cho and Kim [15], which is not plotted in Fig. 6 for simplicity.

As shown by the above comparisons, our present results agree very well with previous analytical results based on a different approach. Also, the present results and previous numerical results obtained by different BEM solutions are in good agreement. It is believed that the newly developed analytical solution should be valid.

Now, we give a generalization of our present solution method. In the submerged-plate region, there are several boundary conditions: the homogeneous Robin condition at the free surface; the homogeneous Neumann condition at the seabed; and the nonhomgenous Robin conditions at the porous-plate surface. When considering the symmetric and antisymmetric potentials, there will be, respectively, a homogeneous Neumann condition and a homogeneous Dirichlet condition at the vertical midline of the plate. All these boundary conditions can be linearly split according to requirement. This process may be rather different for the same problem. Applying the homogenous boundary conditions at the two sides of an interval (no matter if this is in a horizontal or a vertical direction), a series of eigenfunctions with corresponding eigenvalues can be constructed in this interval. Also, the corresponding functions in the normal direction of this interval can be constructed using the Laplace equation. As a result, the velocity potential in this region is obtained. The remaining boundary conditions, which are not used for constructing potentials, are adopted as matching conditions between neighboring potentials. This is how our method works. More problems may be tackled in this way.

5 Conclusions

In this paper, an alternative analytical solution for wave motion over a submerged horizontal porous plate has been developed based on the linear potential theory. The whole fluid domain was divided into four sub-regions by the plate. The velocity potential in each sub-region was split into a symmetric potential and an antisymmetric potential. Each potential above and below the horizontal porous plate was further divided into two parts satisfying appropriate boundary conditions. Then all the velocity potentials were determined by means of the matched-eigenfunction-expansions method. As a result, various hydrodynamic parameters of engineering interest were obtained. The symmetric part of the present solution is also the solution of wave reflection by a submerged horizontal porous plate attached to a vertical solid rear wall.

A convergence examination of the present solution has been carried out. The examination shows that, with suitable truncation number N (number of evanescent modes), identical results can be obtained. Some analytical and BEM results of different researchers have also been used to validate the present solution. The comparisons indicate that the present solution is valid.

The present solution is simple and straightforward without the need for finding the complex roots of the complex wave-dispersion relation. This allows a simpler numerical implementation. In particular, for more significant multi-layer submerged horizontal porous plates, using the traditional analytical method will lead to a very complicated complex dispersion relation. Accurately finding all the roots of such a complex relation is very difficult. But this can be avoided when using our present method. The present solution should be attractive for practical engineering purposes.

A minor drawback of the present solution is that it does not incorporate the singularity near the tip of the plate. An analytical solution for a finite horizontal porous plate that avoids complex roots and incorporates the singularity should be a challenging topic in the future.

The present study may be extended to other scattering objects, such as: a floating elastic plate [34], a submerged elastic plate [35], a submerged flexible porous member [7], a submerged elastic porous plate, multi-layer submerged horizontal porous plates, and so on. This might be subjects for future study.

Acknowledgements This work was financially sponsored by the Natural Science Foundation of China (Grant No. 50909086), State Key Laboratory of Ocean Engineering (Shanghai Jiao Tong University) (Grant No. 0802), and the Natural Science Foundation of Shandong Province (Grant No. Q2008F01). We would like to thank the four anonymous reviewers for their valuable comments, which enhanced the quality of this paper.

Appendix A: Matrix coefficients in Eqs. (51)–(55)

The matrix coefficients in Eqs. (51)–(55) are given by

$$a_{nm}^{S}=\begin{cases}\dfrac{\int_{-d}^{0}Y_n(z)Z_m(z)\mathrm{d}z}{\cos(\lambda_0 b)\int_{-d}^{0}Y_n^2(z)\mathrm{d}z}, & n=0,\\ \dfrac{\int_{-d}^{0}Y_n(z)Z_m(z)\mathrm{d}z}{\int_{-d}^{0}Y_n^2(z)\mathrm{d}z}, & n\neq 0,\end{cases} \tag{A-1}$$

$$b_{n}^{S}=\begin{cases}\dfrac{\int_{-d}^{0}Y_n(z)Z_0(z)\mathrm{d}z}{\cos(\lambda_0 b)\int_{-d}^{0}Y_n^2(z)\mathrm{d}z}, & n=0,\\ \dfrac{\int_{-d}^{0}Y_n(z)Z_0(z)\mathrm{d}z}{\int_{-d}^{0}Y_n^2(z)\mathrm{d}z}, & n\neq 0,\end{cases} \tag{A-2}$$

$$c_{nm}^{S}=\frac{\int_{-h}^{-d}X_n(z)Z_m(z)\mathrm{d}z}{\int_{-h}^{-d}X_n^2(z)\mathrm{d}z}, \tag{A-3}$$

$$d_{n}^{S}=\frac{\int_{-h}^{-d}X_n(z)Z_0(z)\mathrm{d}z}{\int_{-h}^{-d}X_n^2(z)\mathrm{d}z}, \tag{A-4}$$

$$e_{m}^{S}=\begin{cases}-1, & m=0,\\ 0, & m=1,2,\ldots,N,\end{cases} \tag{A-5}$$

$$f_{mn}^{S}=\frac{\tilde{\lambda}_n^S\int_{-d}^{0}Z_m(z)Y_n(z)\mathrm{d}z}{\tilde{k}_m\int_{-h}^{0}Z_m^2(z)\mathrm{d}z}, \tag{A-6}$$

$$g_{mn}^{S}=\frac{\tilde{\mu}_n^S\int_{-h}^{-d}Z_m(z)X_n(z)\mathrm{d}z}{\tilde{k}_m\int_{-h}^{0}Z_m^2(z)\mathrm{d}z}, \tag{A-7}$$

$$h_{mn}^{S}=\frac{\beta_n\sin(\beta_n b)\int_{-d}^{0}Z_m(z)\left[\cosh(\beta_n z)+\omega^2/(\beta_n g)\sinh(\beta_n z)\right]\mathrm{d}z}{\tilde{k}_m\cosh(\beta_n d)\int_{-h}^{0}Z_m^2(z)\mathrm{d}z}, \tag{A-8}$$

$$p_{mn}^{S}=\frac{\beta_n\sin(\beta_n b)\int_{-h}^{-d}Z_m(z)\cosh\beta_n(z+h)\mathrm{d}z}{\tilde{k}_m\cosh(\beta_n s)\int_{-h}^{0}Z_m^2(z)\mathrm{d}z}, \tag{A-9}$$

$$q_{nm}^{S}=\begin{cases}\frac{\tanh(\beta_n s)}{\omega^2/(\beta_n g)-\tanh(\beta_n d)}, & m=n,\\ 0, & m\neq n,\end{cases} \tag{A-10}$$

$$r_{nm}^{S}=\begin{cases}\dfrac{-\mathrm{i}\sqrt{2}k_0 G\int_{-b}^{0}W_n^S(x)\mathrm{d}x}{2[\mathrm{i}k_0 G-\beta_n\tanh(\beta_n s)]\int_{-b}^{0}\left[W_n^S(x)\right]^2\mathrm{d}x}, & m=0,\\ \dfrac{-\mathrm{i}k_0 G\cos(\mu_m s)\int_{-b}^{0}W_n^S(x)\cosh(\mu_m x)\mathrm{d}x}{[\mathrm{i}k_0 G-\beta_n\tanh(\beta_n s)]\cosh(\mu_m b)\int_{-b}^{0}\left[W_n^S(x)\right]^2\mathrm{d}x}, & m\neq 0,\end{cases} \tag{A-11}$$

$$s_{nm}^{S}=\begin{cases}\dfrac{\mathrm{i}k_0 G\left[1-\omega^2/(\beta_n g)\tanh(\beta_n d)\right]}{\mathrm{i}k_0 G-\beta_n\tanh(\beta_n s)}, & m=n,\\ 0, & m\neq n,\end{cases} \tag{A-12}$$

$$t_{nm}^{S}=\begin{cases}\dfrac{\mathrm{i}k_0 G\int_{-b}^{0}W_n^S(x)\cos(\lambda_0 x)\mathrm{d}x}{[\mathrm{i}k_0 G-\beta_n\tanh(\beta_n s)]\cosh(\lambda_0 d)\int_{-b}^{0}\left[W_n^S(x)\right]^2\mathrm{d}x}, & m=0,\\ \dfrac{\mathrm{i}k_0 G\int_{-b}^{0}W_n^S(x)\cosh(\lambda_m x)\mathrm{d}x}{[\mathrm{i}k_0 G-\beta_n\tanh(\beta_n s)]\cos(\lambda_m d)\cosh(\lambda_m b)\int_{-b}^{0}\left[W_n^S(x)\right]^2\mathrm{d}x}, & m\neq 0.\end{cases} \tag{A-13}$$

Appendix B: Matrix coefficients in Eqs. (63)–(67)

The matrix coefficients in Eqs. (63)–(67) are given by

$$a_{nm}^{A} = \frac{\int_{-d}^{0} Y_n(z) Z_m(z)\mathrm{d}z}{\tilde{\lambda}_n^A \int_{-d}^{0} Y_n^2(z)\mathrm{d}z}, \tag{B-1}$$

$$h_{nm}^{A} = \frac{\sin(\beta_m b)\int_{-d}^{0} Y_n(z)\left[\cosh(\beta_m z)+\omega^2/(\beta_m g)\sinh(\beta_m z)\right]\mathrm{d}z}{\tilde{\lambda}_n^A \cosh(\beta_m d)\int_{-d}^{0} Y_n^2(z)\mathrm{d}z}, \tag{B-2}$$

$$b_{n}^{A} = \frac{\int_{-d}^{0} Y_n(z) Z_0(z)\mathrm{d}z}{\tilde{\lambda}_n^A \int_{-d}^{0} Y_n^2(z)\mathrm{d}z}, \tag{B-3}$$

$$c_{nm}^{A} = \frac{\int_{-h}^{-d} X_n(z) Z_m(z)\mathrm{d}z}{\tilde{\mu}_n^A \int_{-h}^{-d} X_n^2(z)\mathrm{d}z}, \tag{B-4}$$

$$p_{nm}^{A} = \frac{\sin(\beta_m b)\int_{-h}^{-d} X_n(z)\cosh\beta_m(z+h)\mathrm{d}z}{\cosh(\beta_m s)\int_{-h}^{-d} X_n^2(z)\mathrm{d}z}, \tag{B-5}$$

$$d_{n}^{A} = \frac{\int_{-h}^{-d} X_n(z) Z_0(z)\mathrm{d}z}{\tilde{\mu}_n^A \int_{-h}^{-d} X_n^2(z)\mathrm{d}z}, \tag{B-6}$$

$$e_{m}^{A} = e_{m}^{S}, \tag{B-7}$$

$$f_{mn}^{A} = \begin{cases} \dfrac{\lambda_0\cos(\lambda_0 b)\int_{-d}^{0} Z_m(z)Y_0(z)\mathrm{d}z}{\tilde{k}_m\int_{-h}^{0} Z_m^2(z)\mathrm{d}z}, & n=0, \\ \dfrac{\lambda_n\int_{-d}^{0} Z_m(z)Y_n(z)\mathrm{d}z}{\tilde{k}_m\int_{-h}^{0} Z_m^2(z)\mathrm{d}z}, & n\neq 0, \end{cases} \tag{B-8}$$

$$g_{mn}^{A} = \begin{cases} \dfrac{\int_{-h}^{-d} Z_m(z)X_0(z)\mathrm{d}z}{\tilde{k}_m\int_{-h}^{0} Z_m^2(z)\mathrm{d}z}, & n=0, \\ \dfrac{\mu_n\int_{-h}^{-d} Z_m(z)X_n(z)\mathrm{d}z}{\tilde{k}_m\int_{-h}^{0} Z_m^2(z)\mathrm{d}z}, & n\neq 0, \end{cases} \tag{B-9}$$

$$q_{nm}^{A} = q_{nm}^{S}, \tag{B-10}$$

$$r_{nm}^{A} = \begin{cases} \dfrac{-\mathrm{i}\sqrt{2}k_0 G\int_{-b}^{0} W_n^A(x)x\mathrm{d}x}{2[\mathrm{i}k_0 G-\beta_n\tanh(\beta_n s)]\int_{-b}^{0}\left[W_n^A(x)\right]^2\mathrm{d}x}, & m=0, \\ \dfrac{-\mathrm{i}k_0 G\cos(\mu_m s)\int_{-b}^{0} W_n^A(x)\sinh(\mu_m x)\mathrm{d}x}{[\mathrm{i}k_0 G-\beta_n\tanh(\beta_n s)]\cosh(\mu_m b)\int_{-b}^{0}\left[W_n^A(x)\right]^2\mathrm{d}x}, & m\neq 0, \end{cases} \tag{B-11}$$

$$s_{nm}^{A} = s_{nm}^{S}, \tag{B-12}$$

$$t_{nm}^{A} = \begin{cases} \dfrac{\mathrm{i}k_0 G\int_{-b}^{0} W_n^A(x)\sin(\lambda_0 x)\mathrm{d}x}{[\mathrm{i}k_0 G-\beta_n\tanh(\beta_n s)]\cosh(\lambda_0 d)\int_{-b}^{0}\left[W_n^A(x)\right]^2\mathrm{d}x}, & m=0, \\ \dfrac{\mathrm{i}k_0 G\int_{-b}^{0} W_n^A(x)\sinh(\lambda_m x)\mathrm{d}x}{[\mathrm{i}k_0 G-\beta_n\tanh(\beta_n s)]\cos(\lambda_m d)\cosh(\lambda_m b)\int_{-b}^{0}\left[W_n^A(x)\right]^2\mathrm{d}x}, & m\neq 0, \end{cases} \tag{B-13}$$

where $\tilde{\lambda}_n^A = \begin{cases} -\sin(\lambda_0 b), & n=0, \\ -\tanh(\lambda_n b), & n\neq 0, \end{cases}$ and $\tilde{\mu}_n^A = \begin{cases} -b, & n=0, \\ -\tanh(\mu_n b), & n\neq 0. \end{cases}$

References

1. Yu XP (2002) Functional performance of a submerged and essentially horizontal plate for offshore wave control: a review. Coast Eng J 44:127–147
2. Yu XP, Chwang AT (1994) Water waves above submerged porous plate. J Eng Mech 120(6):1270–1282

3. Chwang AT, Wu JH (1994) Wave scattering by submerged porous disk. J Eng Mech 120(12):2575–2587
4. Yip TL, Chwang AT (1998) Water wave control by submerged pitching porous plate. J Eng Mech 124(4):428–434
5. Wu JH, Wan ZP, Fang Y (1998) Wave reflection by a vertical wall with a horizontal submerged porous plate. Ocean Eng 25(9):767–779
6. Neves MG, Losada IJ, Losada MA (2000) Short-wave and wave group scattering by submerged porous plate. J Eng Mech 126(10):1048–1056
7. Cho IH, Kim MH (2000) Interactions of horizontal porous flexible membrane with waves. J Waterw Port Coast Ocean Eng 126(5):245–253
8. Wu JH, Chwang AT (2002) Wave diffraction by a vertical cylinder with a porous ring plate. J Eng Mech 128(2):164–171
9. Liu Y, Li YC, Teng B (2007) Wave interaction with a perforated wall breakwater with a submerged horizontal porous plate. Ocean Eng 34:2364–2373
10. Liu Y, Li YC, Teng B et al (2008) Wave motion over a submerged breakwater with an upper horizontal porous plate and a lower horizontal solid plate. Ocean Eng 35:1588–1596
11. Kee ST (2009) Submerged plate breakwater composed of horizontal porous plate and slightly inclined solid plate. Int J Offshore Polar Eng 19(1):42–45
12. Yueh CY, Chuang SH (2009) Wave scattering by a submerged porous plate wave absorber. In: Proceedings of the 19th international offshore and polar engineering conference, Osaka, Japan, vol 3, pp 1167–1173
13. Bao W, Kinoshita T, Zhao F (2009) Wave forces acting on a semi-submerged porous circular cylinder. Proc IMechE Part M 223:349–360
14. Park WT, Lee SH, Kee ST et al (2005) Submerged porous plate wave absorber. In: Proceedings of the 15th international offshore and polar engineering conference, Seoul, Korea, vol 3, pp 595–599
15. Cho IH, Kim MH (2008) Wave absorbing system using inclined perforated plates. J Fluid Mech 608:1–20
16. Evans DV, Peter MA (2010) Asymptotic reflection of linear water waves by submerged horizontal porous plates. J Eng Math (in press). doi:10.1007/s10665-009-9355-2
17. McIver P (1998) The dispersion relation and eigenfunction expansions for water waves in a porous structure. J Eng Math 34:319–334
18. Mendez FJ, Losada IJ (2004) A perturbation method to solve dispersion equations for water waves over dissipative media. Coast Eng 51:81–89
19. Chang HK, Liou JC (2006) Solving wave dispersion equation for dissipative media using homotopy perturbation technique. J Waterw Port Coast Ocean Eng 132(1):28–35
20. Yu XP (1995) Diffraction of water waves by porous breakwaters. J Waterw Port Coast Ocean Eng 121(6):275–282
21. Chwang AT (1983) A porous-wavemaker theory. J Fluid Mech 132:395–406
22. Isaacson M, Premasiri S, Yang G (1998) Wave interactions with vertical slotted barriers. J Waterw Port Coast Ocean Eng 124(3):118–126
23. Tao LB, Song H, Chakrabarti S (2009) Wave interaction with a perforated circular breakwater of non-uniform porosity. J Eng Math 65:257–271
24. Teng B, Zhang XT, Ning DZ (2004) Interaction of oblique waves with infinite number of perforated caissons. Ocean Eng 31:615–632
25. Mei CC, Black JI (1969) Scattering of surface waves by rectangular obstacles in waters of finite depth. J Fluid Mech 38:499–511
26. Lee JF (1995) On the heave radiation of a rectangular structure. Ocean Eng 22:19–34
27. Lee JF, Liu CC (1995) A new solution of waves passing a submerged porous structure. In: Proceedings of the 17th ocean engineering conference, Taiwan, China, pp 593–606 (in Chinese with English abstract)
28. Lan YJ, Hsu TW, Lai JW et al (2009) Bragg scattering of waves propagating over a series of poro-elastic submerged breakwaters. In: Proceedings of the 19th international offshore and polar engineering conference, Osaka, Japan, vol 3, pp 1180–1187
29. Linton CM, McIver P (2001) Handbook of mathematical techniques for wave/structure interactions. Chapman & Hall/CRC, Boca Raton
30. Porter R, Evans DV (1995) Complementary approximations to wave scattering by vertical barriers. J Fluid Mech 294:155–180
31. Porter R (1995) Complementary method and bounds in linear water waves. Doctoral thesis, University of Bristol
32. Mandal BN, Kanoria M (2000) Oblique wave-scattering by thick horizontal barriers. J Offshore Mech Arct Eng 122:100–108
33. Martins-rivas H, Mei CC (2009) Wave power extraction from an oscillating water column at the tip of a breakwater. J Fluid Mech 626:395–414
34. Peter MA, Meylan MH, Chung H (2004) Wave scattering by a circular elastic plate in water of finite depth: a closed form solution. IJOPE 14(2):81–85
35. Hassan M, Meylan MH, Peter MA (2009) Water-wave scattering by submerged elastic plates. Q J Mech Appl Math 62(3):321–344